Modeling Analysis of the Swell and Wind-Sea Climate in the Salish Sea

Zhaoqing Yang[1,2]*, Gabriel García-Medina[1], Wei-Cheng Wu[1], Taiping Wang[1], L. Ruby Leung[3], Luca Castrucci[1], and Guillaume Mauger[4]

[1]Marine Sciences Laboratory, Pacific Northwest National Laboratory, Seattle, WA, U.S.A

[2]Department of Civil and Environmental Engineering, University of Washington, Seattle, WA, U.S.A

[3]Atmospheric Sciences and Global Change, Pacific Northwest National Laboratory, Richland, WA, U.S.A

[4]Climate Impact Group, University of Washington, Seattle, WA, U.S.A

* Corresponding author: zhaoqing.yang@pnnl.gov

Highlights:

- A high-resolution modeling study was carried out to systematically characterize wave climate in Salish Sea.
- Spatial resolution of wind forcing plays an important role in the accuracy of wave hindcast in estuaries with interconnected sub-basins.
- Sea state is dominated by swell in the entrance of Salish Sea and dominated by wind-sea in the Strait of Georgia and Puget Sound.

- Sea state shows strong seasonal variations in the Strait of Juan de Fuca and the Strait of Georgia but little seasonality in Puget Sound.

Key words: wave climate, numerical modeling, Salish Sea, SWAN, WW3, WRF

ABSTRACT

Accurate model hindcast of wave climate in complex estuarine systems is challenging because high-resolution wave models and wind forcing are required. In this study, a modeling approach using the unstructured-grid Simulating WAves Nearshore and a wind product from a high-resolution regional Weather Research and Forecasting hindcast was used to simulate the swell and wind-sea climate in the Salish Sea, a large estuary with many interconnected waterways on the Pacific Northwest coast of North America. The model hindcast was validated with observed data at four wave buoys. Spatial distribution and seasonal variations in wave climate in the Salish Sea were analyzed. Of the three major basins in the Salish Sea, the Strait of Juan de Fuca has the largest waves and is dominated by swells propagated from the Pacific Ocean. Significant wave heights in the Strait of Georgia have spatial and seasonal distribution patterns similar to those found in the Strait of Juan de Fuca. Waves in Puget Sound are small and primarily dominated by the wind-sea climate. Strong seasonal variations are observed in the Strait of Juan de Fuca and Strait of Georgia, but there is little seasonality of wave climate in Puget Sound. The high-resolution wave hindcast conducted in this study provides a comprehensive and important data set for better understanding the role of wave climate in coastal processes and natural hazards assessment in the Salish Sea.

1 Introduction

The Salish Sea, which consists of the Strait of Juan de Fuca (SJDF), Strait of Georgia (SoG), and Puget Sound, is an inland sea on the Pacific coast bordered by the U.S. state of Washington (WA) and British Columbia (BC), Canada (FIG. 1). The Salish Sea is the second largest estuary in the U.S. and its coast hosts major U.S. and Canadian cities and ports such as Olympia, Seattle, Tacoma, Victoria, and Vancouver. The Salish Sea connects to the Pacific Ocean via the SJDF that separates Washington State and Vancouver Island and via Johnstone Strait at the northern end of Vancouver Island. The Pacific Northwest (PNW) coast, including Washington, Oregon, and northern California, is subject to an energetic wave climate caused by westerly winds at mid-latitudes blowing over the northern Pacific Ocean, and the WA and BC coasts are in the path of the dominant tracks for winter extratropical storms (Allan and Komar, 2002; Harr et al., 2000; Kita et al., 2018; Martin et al., 2001; Mass and Dotson, 2010; Mesquita et al., 2010). Therefore, the PNW coast is one of the top coastal regions in U.S. identified for wave energy development (EPRI, 2011). There are concerns about coastal flooding induced by large waves and storm surge during extreme storm events. Despite the economic and strategic importance of the Salish Sea, no detailed studies of the wave climate have been conducted there, either using numerical modeling or field measurements.

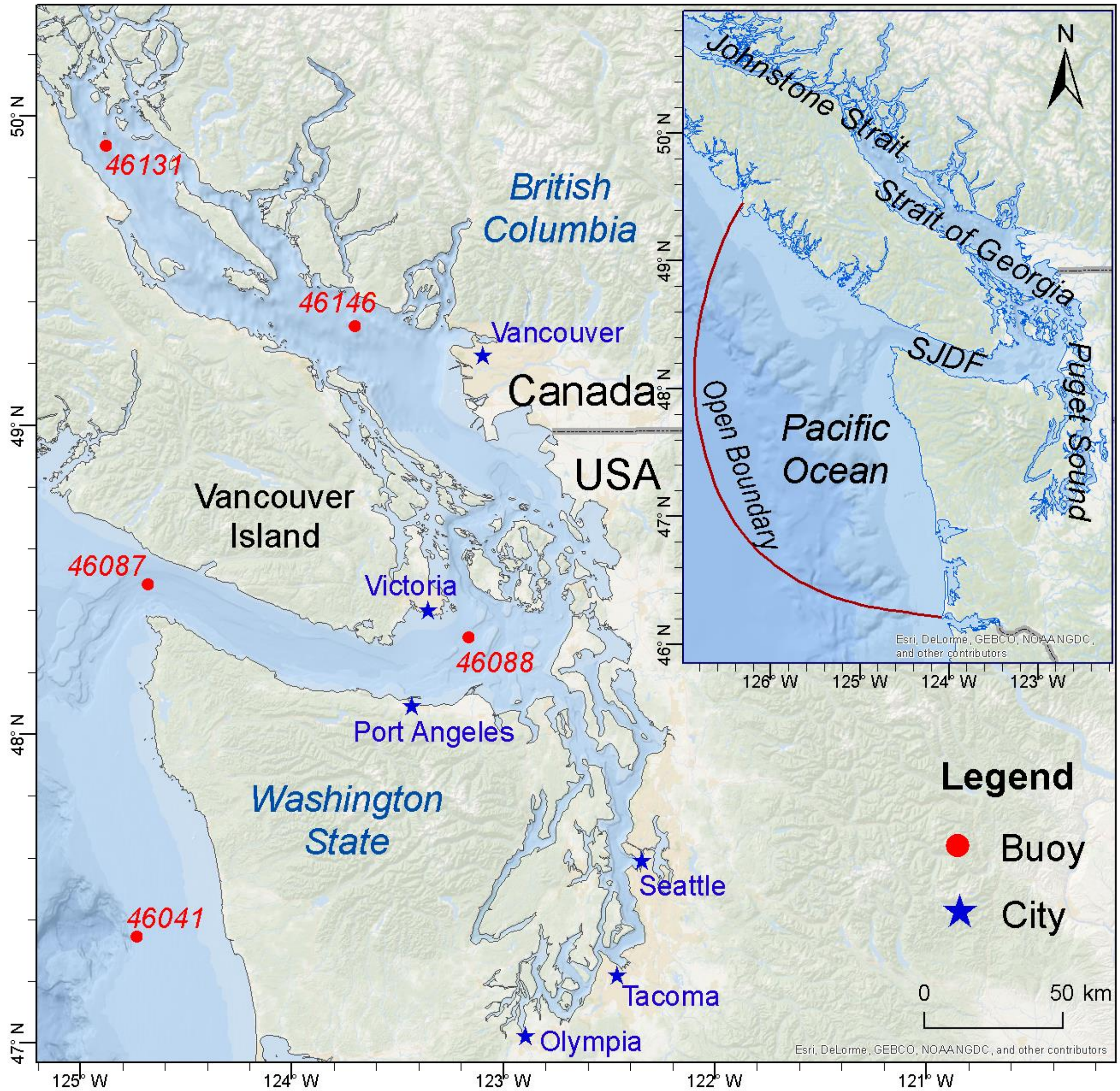

FIG. 1. The Salish Sea and surrounding regions. Buoys used for data model comparisons are shown as dots. The red line indicates the wave model open boundary and color contours show the bathymetry. The Strait of Juan de Fuca and Strait of Georgia are abbreviated as SJDF and SoG, respectively.

Wave climate in nearshore regions highly depends on remote incoming wave characteristics and can vary greatly within a region because of the wind forcing and complexity of the local geometry, including bathymetry, coastline characteristics, and presence of sub-basins. Better understanding of the process of wave energy growth and dissipation in a large estuarine system like the Salish Sea is important, not only for characterizing the wave energy resource, but also for minimizing the impact of coastal hazards and restoring coastal ecosystems. Although many wave modeling studies have been conducted in regional oceans, coastal bays, and estuaries (Albarakati and Aboobacker, 2018; Beudin et al., 2017; Bolanos-Sanchez et al., 2007; Chen et al., 2003; Cheng et al., 2015; Dupuis and Anis, 2013; Gorman and Neilson, 1999; Mulligan et al., 2008; Nayak et al., 2013; Rusu et al., 2011b; Semedo et al., 2015; Xu et al., 2005), few studies have focused on wave transformation and the effect of wind forcing at an estuarine basin scale (Alari et al., 2008; Bento et al., 2015; Lin et al., 2002; Niroomandi et al., 2018; Rusu et al., 2011a).

To date, little is known about how wave energy grows and dissipates as swells from the Pacific Ocean propagate into the Salish Sea. In this study, a high-resolution wave hindcast was performed using state-of-the-art modeling techniques to assess the wave climate in the Salish Sea and its sub-basins. Section 2 describes the model implementation, and the results are presented and discussed in Section 3. Section 3.1 presents data model comparisons with an emphasis on the sensitivity of the wave model to the wind input. Sections 3.2 and 3.3 describe the respective spatial and seasonal characteristics of the wave climate in the Salish Sea. A summary and concluding remarks follow in Section **Error! Reference source not found.**.

2 Methods

2.1 Salish Sea Wave Model

In this study, the third-generation phase-averaged wave model, Simulating WAves Nearshore (SWAN) (SWAN Team, 2017) was used to simulate the wave climate in the Salish Sea. SWAN is one of the most widely used models and has been implemented successfully in many nearshore and shallow-water applications (e.g., O'Dea et al., 2018; Wu et al., 2018). SWAN solves the following action balance equation:

$$\frac{\partial \mathrm{N}}{\partial \mathrm{t}} + \frac{\partial c_{gx} N}{\partial x} + \frac{\partial c_{gy} N}{\partial y} + \frac{\partial c_{\theta} N}{\partial \theta} + \frac{\partial c_{\sigma} N}{\partial \sigma} = \frac{1}{\sigma}(\mathrm{S_{in}} + \mathrm{S_{ds}} + \mathrm{S_{nl}} + \mathrm{S_{bot}} + \mathrm{S_{brk}})$$

where the left-hand side represents the total derivative of the wave action (N) in spatial (x,y), directional (θ), and frequency (σ) space. The velocity of propagation in each dimension is represented by c. The right-hand side represents the sinks and sources of energy; S_{in} represents the wave growth due to wind, using the Janssen (1989, 1991) method in combination with the linear growth function of Cavaleri and Rizzoli (1981); S_{ds} represents the dissipation of energy due to whitecapping as described by Komen et al. (1984); the non-linear quadruplet wave interactions (S_{nl}) are modeled using the discrete interaction approximation method of Hasselmann et al. (1985); and the bottom friction (S_{bot}) and depth-induced wave breaking (S_{brk}) are modeled using the Hasselmann et al. (1973) and Battjes and Janssen (1978) formulations. The default parameters are used for all the source terms.

Because of the complex geometry of the Salish Sea, especially the presence of several sub-basins in Puget Sound, the unstructured-grid version of SWAN (UnSWAN) was used in this study. The unstructured-grid approach allows one to focus resources nearshore and in areas of complex geometry, while relaxing the model resolution over deeper waters. The unstructured-grid modeling approach has been used successfully to simulate waves in the PNW (Cheng et al., 2015; Robertson et al., 2014; Wu et al., 2018). The wave model grid for the Salish Sea was built based on the high-resolution unstructured-grid for the Salish Sea hydrodynamic and transport model (Wang and Yang, 2017; Yang and Khangaonkar, 2010; Yang and Wang, 2015). The model open boundary is extended 170 km out to the inner shelf from 49°29'9" N in the north to 46°16'40" N in the south, such that propagation of incoming swells can be properly simulated (García-Medina et al., 2013). The model grid has a total of 120,073 vertices and 217,388 elements. The grid element area varies from 41,400,000 m^2 at the offshore boundary to 100 m^2 at the shoreline in the Salish Sea, which roughly translates to a 10 km grid resolution at the offshore boundary and a 10 m grid resolution at the major estuarine mouths in Puget Sound, such as Skagit River and Snohomish River in Whidbey Basin, the Skokomish River in Hood Canal, and the Puyallup River in the South Sound. The model resolution at the entrance to the SJDF is approximately 1 km with a total of 22 grid points in the across-channel direction. The offshore boundary of the grid extends approximately 165 km from the entrance to the SJDF. The bathymetry in Puget Sound was interpolated from the combination of the National Oceanic and Atmospheric Administration's (NOAA's) 1/3 arc-second Digital Elevation Model (DEM) of Puget Sound (Carignan et al., 2014) and the University of Washington's combined bathymetry and topography DEM of Western Washington (Finlayson, 2005). The bathymetry in the outer coastal region was obtained from NOAA's ETOPO1 Global Relief Model, which is a 1-

arc-minute global relief model of Earth's surface that integrates land topography and ocean bathymetry (Amante and Eakins, 2009).

The UnSWAN model was executed in time-dependent mode with a time step of 10 minutes. The wave spectrum was discretized in frequency space using 29 logarithmically spaced bins from 0.035 to 0.505 Hz, which covers the expected range of waves that reach the U.S. West Coast from distant sources and is also able to capture local wave generation. In directional space, 24 equally spaced bins are used, giving a directional resolution of 15 degrees. Significant wave height (H_s), peak wave period (T_p), mean wave period based on the first spectral moment (T_{m01}), mean wave direction (D_m), and peak wave direction (D_p) are collected at hourly intervals across the entire computational grid.

The effect of current is not considered in the model configuration even though tidal current is strong in the Salish Sea, because the focus of the study was to evaluate the wave energy growth and dissipation in the Salish Sea. Similarly, the effect of river discharge was also not considered in this study.

2.2 Open Boundary Forcing

The wave boundary conditions for the Salish Sea SWAN model were forced by hourly spectral output from a three-level nested WAVEWATCH III model (WW3), developed by Yang et al. (2018) as part of a wave resource characterization study on the U.S. West Coast. WW3 is a third-generation phase-average wave model developed by NOAA's National Center for Environmental Prediction (NCEP) (Tolman and WAVEWATCH III Development Group, 2014). It solves the same spectral wave action balance equation as SWAN. NOAA NCEP currently conducts a wave forecast four times a day using multigrid WW3 for the global and regional oceans, including the Arctic Ocean, Northwest Atlantic, East Pacific, Alaskan Coast, U.S. West Coast, and Gulf of Mexico (http://polar.ncep.noaa.gov/waves/implementations.php). WW3 has been widely used and validated not only at a global scale but also at shelf and coastal bay scales (Anselmi-Molina et al., 2012; Crosby et al., 2017; Crosby et al., 2016; García-Medina et al., 2014; Sartini et al., 2018; Umesh et al., 2018; Yang et al., 2017; Yang et al., 2018). The three-level nested WW3 includes a 30-arc-minute resolution global domain and two nested regional domains with 6-arc-minute and 1-arc-minute resolutions. The 1-arc-minute resolution model covers the entire U.S. West Coast, including the states of Washington, Oregon, and California, and extends offshore up to the 200 nautical miles Exclusive Economic Zone. In this study, the three-level nested WW3 model used the same model configurations as UnSWAN in both the frequency and spectral domains. For more detailed information about the 1-arc-minute WW3 model configuration and validation for the U.S. West Coast, the readers are referred to the previous studies (Yang et al., 2017; Yang et al., 2018).

2.3 Buoy Data for Model Validation

One of the challenges for wave model hindcasting in the Salish Sea is the lack of high-quality wave data for model validation, which is an important step in assessing the accuracy of model performance and increasing the confidence in model applications. In particular, to evaluate the model performance in simulating wave energy growth, dissipation in swell and wind-sea climate, observed spectral wave data with long-term records, and reasonable spatial coverage for the model domain are needed. However, few long-term measurement stations exist in the Salish Sea. A total of five buoys are in the UnSWAN domain, as shown in FIG. 1. The water depth and operation details are provided in TABLE 1. The National Data Buoy Center (NDBC) operates three wave buoys, 46041 on the Pacific coast of Washington State, 46087 near the entrance of the SJDF, and 46088 in the eastern SJDF, while the Department of Fisheries and Oceans (DFO) Canada operates two buoys in the SoG. However, wave direction data are not available at the DFO buoys. Further QA/QC analysis indicated that the quality of the wave period data at DFO buoys is also very poor. Therefore, wave period and direction data at the DFO buoys were not used in the model validation. These buoys are located in water depths ranging from 14 to 261 m, covering a wide range of conditions from deep to shallow waters, and thus giving a representative sample of model performance. No measurements are taken in the Puget Sound. Although these buoys do not provide comprehensive spatial coverage, they can be used to validate and calibrate wave models, which can be used to explore the wave characteristics in the entire Salish Sea.

TABLE 1. Ground truth stations inside the Salish Sea.

Buoy ID	**Coordinates**	**Depth (m)**	**Agency**	**Operation**
46041	47°21’10” N, 124°44’30” W	128	NOAA	Since 06/1987
46087	48°29’35” N, 124°43’35” W	261	NOAA	Since 07/2004
46088	48°20’01” N, 123°09’53” W	114	NOAA	Since 09/2004
46131	49°54’36” N, 124°59’24” W	14	DFO	Since 10/1992
46146	49°20’24” N, 123°43’48” W	42	DFO	Since 03/1992

2.4 Wind Forcing

Given the complex geometry of the Salish Sea and its relative sheltering from the open coast, especially in Puget Sound, high-quality wind forcing is particularly important for accurately simulating wave climate in the Salish Sea. In this study, Climate Forecast System Reanalysis (CFSR) (Saha et al., 2010) was used to drive the three-level global-regional WW3 model. CFSR provides hourly wind field, among many other meteorological variables, at 30-arc-minute (~35 km in the zonal direction at 50° N latitude) grid resolution with global coverage from 1979 to the present. CFSR wind has also been widely used in wave hindcasts at global scales and in many open coastal regions around the world (Akpinar et al., 2016; Campos et al., 2018; Campos and Soares, 2016; Lavidas et al., 2017; Morim et al., 2016; Stopa and Cheung, 2014; Yang et al., 2018).

However, at 30-arc-minute resolution, CFSR provides a limited number of data points in the Salish Sea. In particular, there are no CFSR data points in Puget Sound and only a few points in the SJDF and SoG (FIG 2a). Clearly, the grid resolution of CFSR is insufficient to provide accurate surface wind forcing to drive wave hindcasting in the Salish Sea. Therefore, a higher-resolution wind product is needed. A regional climate simulation using the Weather Research and Forecasting (WRF) model (Skamarock et al., 2008) was performed by the Pacific Northwest National Laboratory over the western U.S. at a grid spacing of 6 km (Gao et al., 2017). The WRF-PNNL simulation was driven by large-scale boundary conditions from the North American Regional Reanalysis (Mesinger et al., 2006) for the period of 1980–2015. More details about the WRF-PNNL simulation, including the choice of physics parameterizations, which follow Gao et al. (2017), and comparison of observed and simulated precipitation are provided by Chen et al. (2018).

Surface variables such as 10 m winds, 2 m surface air temperature, and precipitation are archived at hourly intervals. The distribution of the WRF-PNNL grid points in the Salish Sea basin is also shown in FIG 2a. Compared to the CFSR grid resolution, the WRF-PNNL model has much higher resolution and provides better coverage in the Salish Sea. Scatter plots of CFSR and WRF-PNNL simulated winds and observed data at buoy stations 46131, 46146, and 46088 in the Salish Sea are presented in FIG 2b-g. Compared to the CFSR simulation of winds, the WRF-PNNL simulation captured more spatiotemporal variability of winds because it was run at a higher spatial and temporal resolution, which is important for simulating winds in the orographically complex region of the Salish Sea. CFSR significantly underpredicted sea-surface wind at all three buoy stations, while the WRF-PNNL model results showed reasonable agreement with observed data.

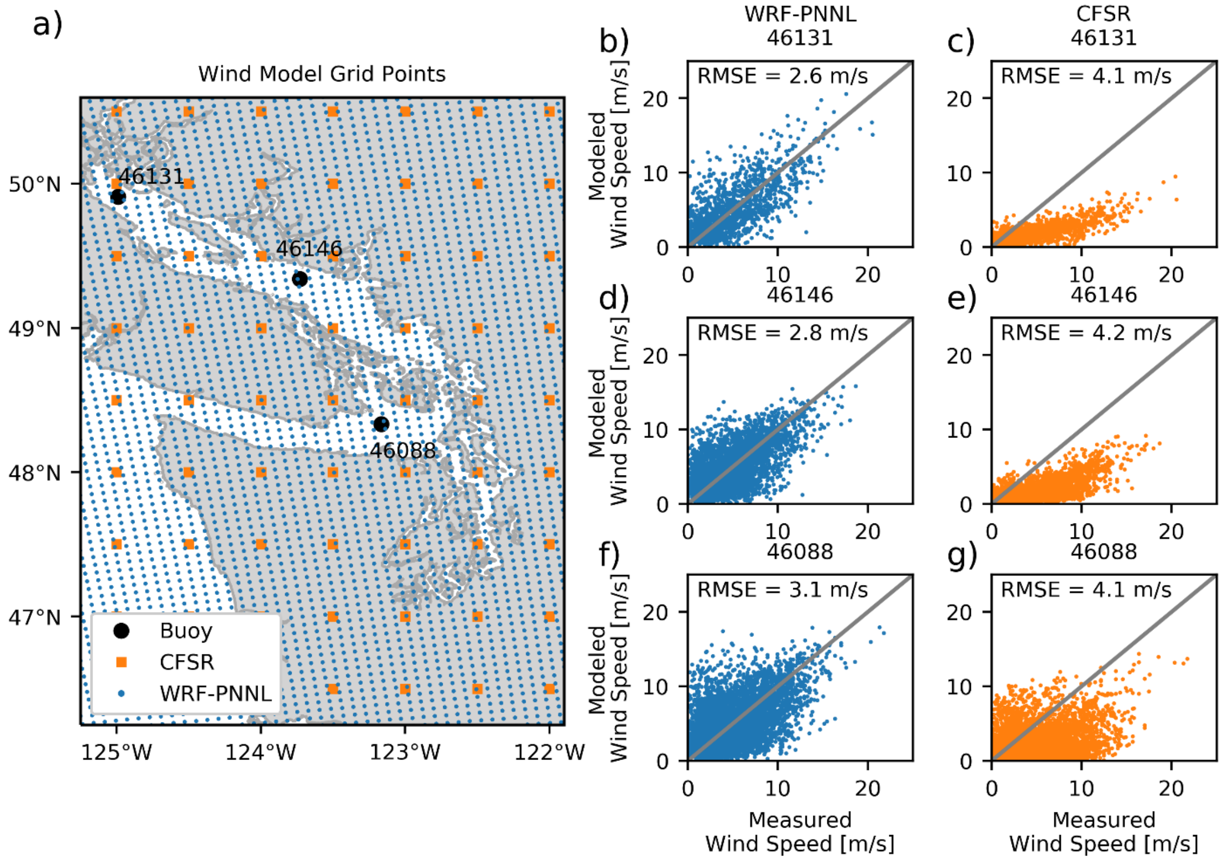

FIG 2. (a) Comparison of the grid resolution of the CFSR and WRF-PNNL models. (b-g) Model-data comparison for wind speed at buoy locations.

To further assess the influence of wind forcing on wave hindcasting in the Salish Sea, a sensitivity model run for year 2015 was conducted using WRF-PNNL and CFSR simulated winds. Model performance for simulating significant wave height (H_s) with two different wind-forcing products was compared among buoy stations 46131, 46146, and 46088, as shown in the scatter plots (FIG. 3a-c). Clearly, simulated significant wave height is much better in all three stations in the Salish Sea when forced by the WRF-PNNL winds compared to those forced by CFSR. In general, the waves are significantly underestimated when the model is forced by CFSR, as could have been expected from the comparison of wind speeds at these buoys (FIG 2). A set of error statistic metrics, including the root-mean-square-error (RMSE), the percent error (PE), the scatter index (SI), the bias, and the linear correlation coefficient (R), were calculated to quantify the model's performance. The formulations of these error statistical parameters are provided in Appendix A. As indicated in TABLE 2, all error statistical parameters for simulated significant wave height forced by WRF-PNNL wind were better than those forced by CFSR wind. The simulated significant wave height using the WRF-PNNL wind forcing is improved in the Salish Sea, resulting in a decrease in the bias in absolute terms.

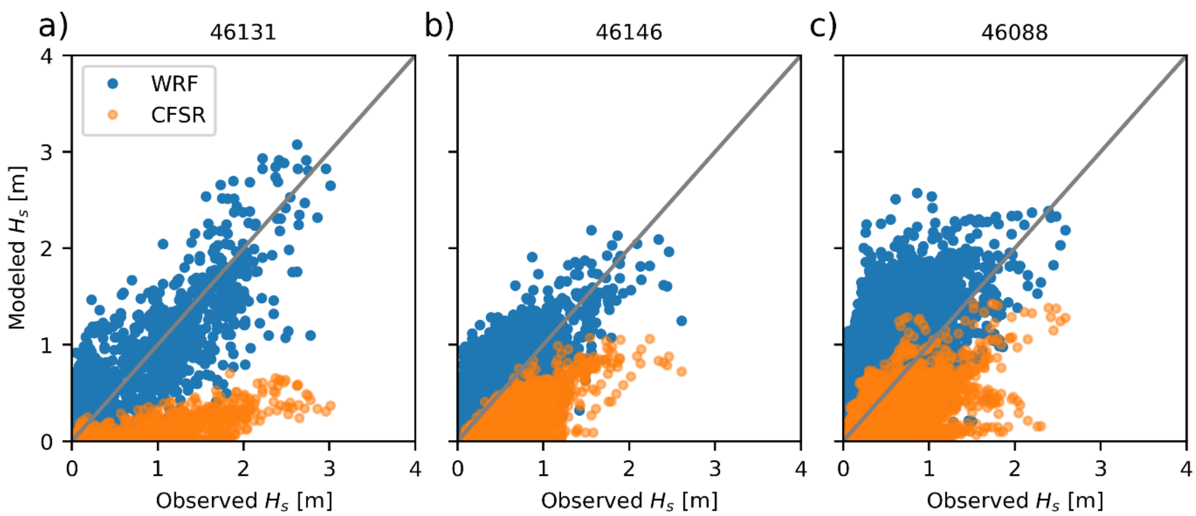

FIG. 3. Comparisons of simulated and observed H_s when forced by WRF and CFSR for year 2015.

Local wind-wave generation was also evaluated by computing the percent of time during 2015 that the waves were above a specific threshold of significant wave height, such as 10 cm. At buoy 46088 in the SJDF, waves above this threshold were 89%, 89%, and 42% of the time based respectively on observed data, SWAN-WRF-PNNL and SWAN-CFSR results. As shown in FIG. 3, most of the time the SWAN-CFSR combination significantly under-predicts the wave heights. In the SoG, the model behavior is similar;

for buoy 46146, 86%, 74%, and 17% of the time the waves exceed the threshold, while for buoy 46131, the threshold is exceeded 40%, 44%, and 11% of the time. Consistent results were found when different threshold values were used—from 5 cm to 30 cm in 5 cm increments. The threshold exceedance analysis suggests that the time periods during which waves are generated in the Salish Sea are well captured by the SWAN model forced by WRF-PNNL wind. However, at least half of the time periods are missed when the wave model is forced by CFSR wind. Therefore, based on the assessment of wave model performance in simulating significant wave height using both CFSR and WRF-PNNL wind products, WRF-PNNL wind is adequate to drive the basin-scale wave model to simulate swell and wind-sea climate in the Salish Sea.

TABLE 2. UnSWAN model performance for simulating H_s when forced by CFSR and WRF-PNNL winds. Statistics are based on results for 2015.

Parameter	**Buoy**	**Wind Model**	**RMSE**	**PE (%)**	**SI**	**Bias**	**R**
H_s (m)	46088	WRF-PNNL	0.33	64.5	0.93	0.14	0.69
		CFSR	0.33	-51.1	0.92	-0.22	0.53
	46131	WRF-PNNL	0.23	9.0	0.74	-0.01	0.89
		CFSR	0.52	-91.7	1.68	-0.27	0.80
	46146	WRF-PNNL	0.24	16.8	0.63	0	0.73
		CFSR	0.40	-89.9	1.05	-0.32	0.68

3 Results and Discussion

3.1 Model Validation

To validate the model, the model simulation period should be selected based on the availability of wave buoy data and wind forcing. Although the two DFO buoys (46131 and 46146) have data records back to 1992, the two NDBC buoys (46087 and 46088) in the SJDF did not start full-year measurements until 2005, as shown in TABLE 1. The WRF-PNNL simulations end in 2015. Therefore, the number of years with full-year data records and wind forcing are 11 years, from 2005 to 2015. In balancing with the computational cost and the period of high-resolution wave hindcast, a 5-year simulation period was determined, from 2011 to 2015. To confirm that a 5-year simulation is sufficient to characterize the overall wave climate in the Salish Sea, the significant wave height distribution, based on observed data at buoys 46087 and 46088 for the entire data record (2004–present) and the simulation period 2011–2015, was compared and analyzed (FIG. 4a-b). The vast majority of the wave heights measured at both buoys were simulated in the present study, indicating 2011–2015 is a representative period for the mean climatology of the region.

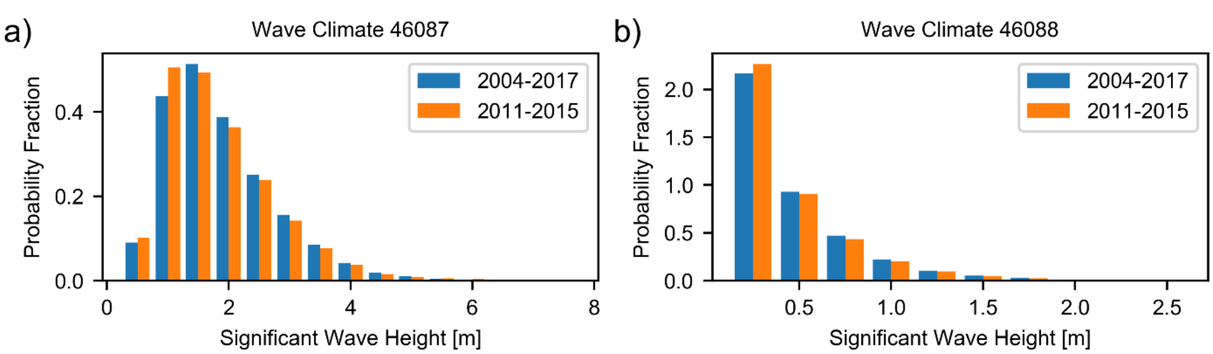

FIG. 4. Probability density function of significant wave height for the full record (blue) and the modeled period (orange) at buoys 46087 (a) and 46088 (b).

Model performance is assessed by comparing the hindcast results with measurements derived from buoys inside the model domain. For all the simulations, bulk wave parameters are stored at the top of the hour across the computational domain. Model results are interpolated to the time of the measurements to perform the comparisons. FIG. 5 shows the time-series comparisons of modeled and measured significant wave height at the five buoy locations for the second half of 2015. Overall, model results are in good agreement with the data, especially at the locations outside of the Salish Sea (FIG. 5a, b). The wave climate is well captured in the model, in terms of wave magnitude and variability at all locations. Waves are much larger along Washington's Pacific Coast and at the SJDF entrance (FIG. 5a, b). However, waves decrease significantly and become more variable at shorter time scales as locations move inland (FIG. 5c-e). To better understand the spatial variation of wave height distribution in the Salish Sea, FIG. 6 shows a snapshot of significant wave height over the model domain during a storm event that brought 9 m waves to the entrance of the SJDF. The wave height is reduced drastically over the length of the SJDF from 9 m on the western side to about 2 m on the eastern side of the SJDF for a distance of about 150 km. In the SoG and Puget Sound, waves are mostly below 2 m and the small spatial variation in wave height is mainly subject to local wind action.

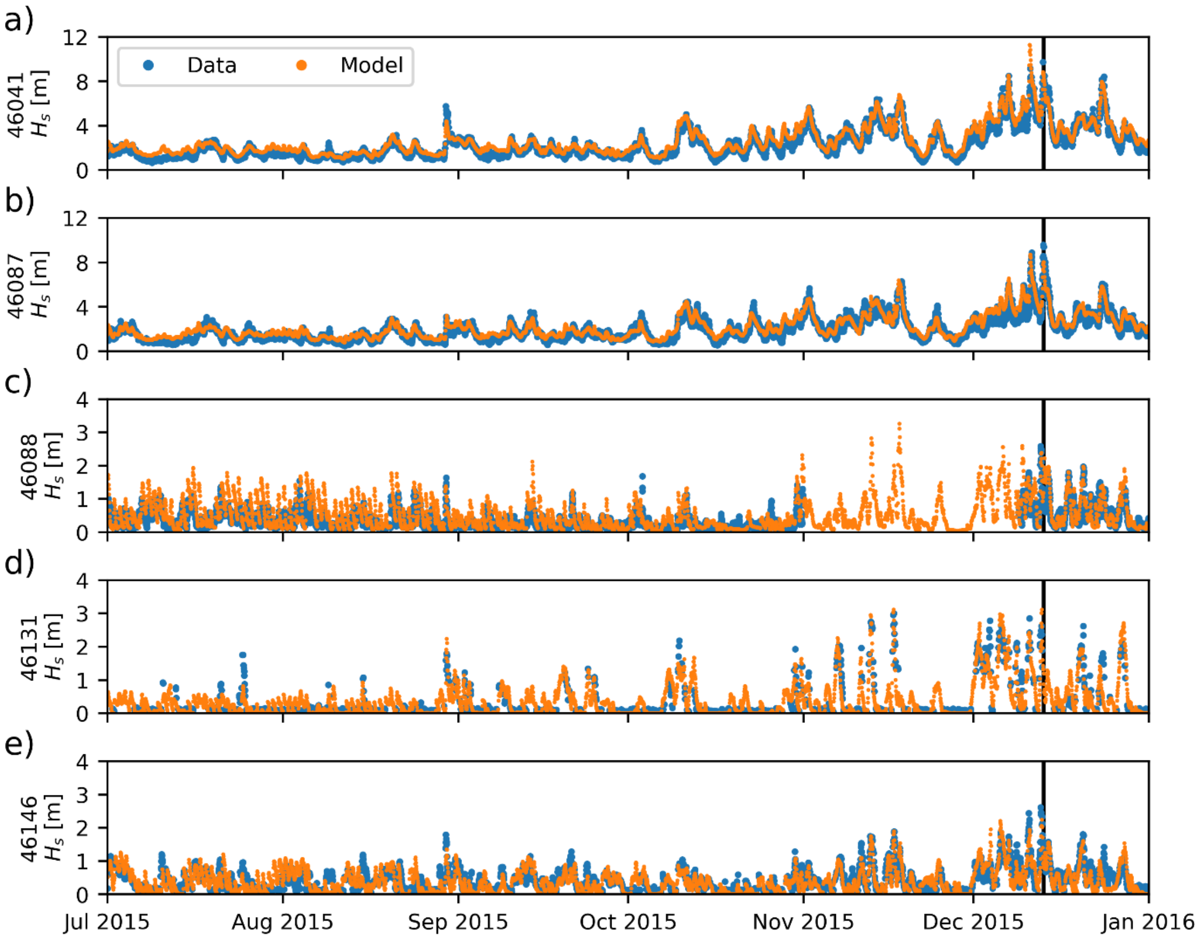

FIG. 5a-e. Comparison of simulated and observed Hs at all stations inside the model domain for the second half of 2015. Note: the vertical scale for c-e is smaller than a-b. Vertical black line indicates the conditions at 10:00 on 13 December 2018, shown spatially in FIG. 6.

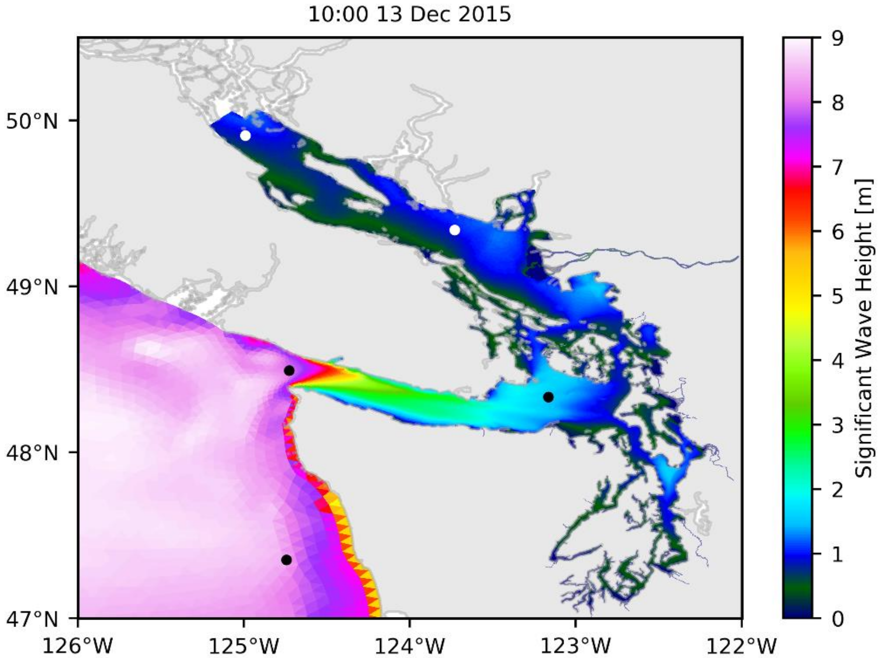

FIG. 6. Spatial distribution of significant wave height during a storm event at 10:00 on 13 December 2018. Buoy locations are shown as black and white dots for reference; they are identified in FIG. 5.

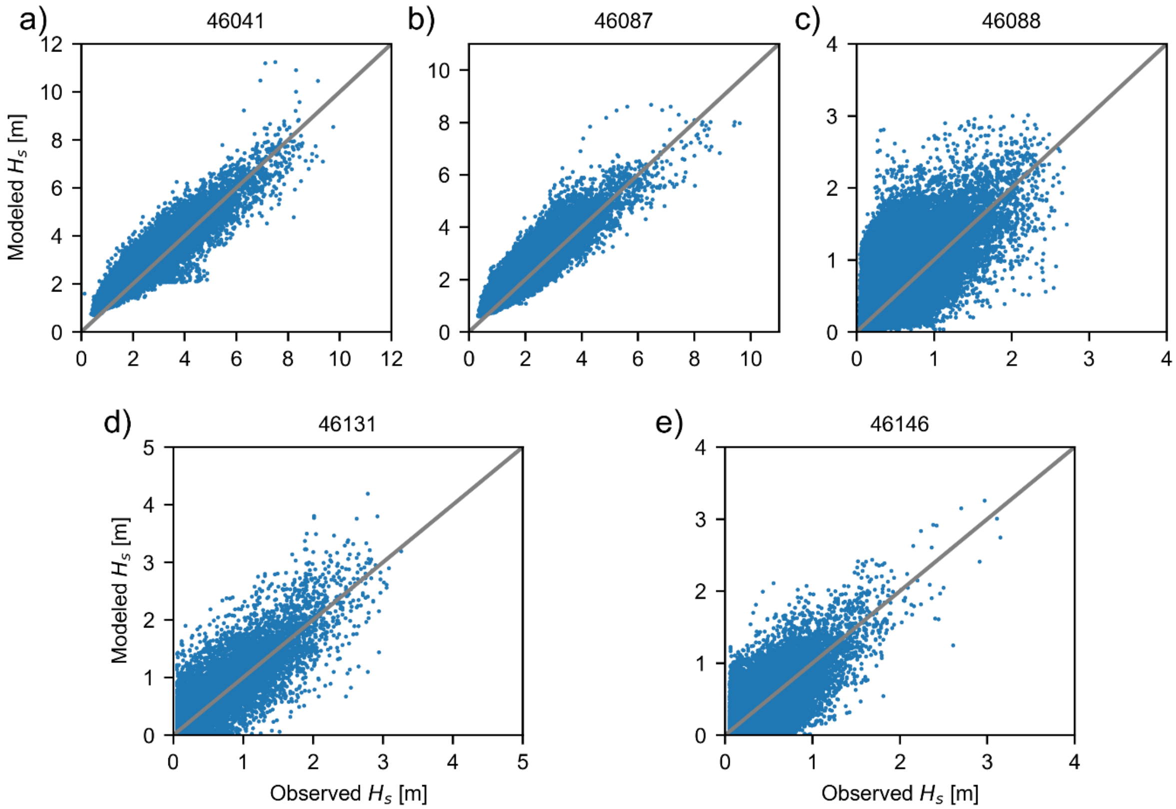

FIG. 7a-e. Comparisons of significant wave height at buoy locations on the Washington outer coast and in the Salish Sea.

Model performance was also evaluated using a set of error statistics, which are defined in Appendix A. TABLE 3 shows that the model performance for open ocean stations is similar to other open ocean wave studies: $\mathrm{SI} \approx 0.2$ and $\mathrm{R} \gtrsim 0.9$ (e.g., (García-medina et al., 2014; Wu et al., 2018). The non-dimensional metrics show a reduction in model skill inside the Salish Sea, particularly at buoy 46088, where sea state is the most complicated because it is influenced by wind forcing from different directions. The reduction in model skill might also be partially due to poorer wind model performance, as shown in FIG 2f. In the eastern SJDF, UnSWAN tends to overestimate the waves, but the model performance is within the range of previously published results (García-Medina et al., 2014; Guillou and Chapalain, 2015; Hanson et al., 2009; Yang et al., 2017).

TABLE 3. Error statistics for UnSWAN model performance. Measurements of wave period from the DFO buoys are not realistic and are therefore not included in the model performance assessment. SI and PE are not reported for peak wave direction because division by the mean is not meaningful in this case. Negative and positive bias represent counterclockwise and clockwise model shifts, respectively. The absolute difference between the measurements and model results was kept under 180°.

Parameter	**Buoy**	**RMSE**	**PE (%)**	**SI**	**Bias**	**R**
	46041	0.27	20.4	0.23	0.27	0.94
	46087	0.47	20.1	0.26	0.26	0.91
H_s (m)	46088	0.35	67.8	0.89	0.15	0.69
	46131	0.27	22.5	0.73	0.04	0.86
	46146	0.24	21.5	0.68	0.01	0.73
	46041	1.45	16.3	0.21	1.11	0.86
T_{m01} (s)	46087	1.32	11.4	0.18	0.78	0.79
	46088	1.97	4.3	0.52	0.06	0.23
	46041	24.85	-	-	-6.29	0.67
D_p (°)	46087	23.65	-	-	1.83	0.59
	46088	48.57	-	-	3.49	0.72

3.2 Spatial Characteristics of Sea State

To understand the general sea-state distribution in the Salish Sea, wave roses were generated using the 5-year model hindcast data at selected locations throughout the Salish Sea (FIG. *8*). Wave roses show the frequency and relative height (percentiles) of waves coming from particular directions. The wave direction is defined as the incoming wave direction. The maximum significant wave height during the 5-year simulation period at each location is listed next to the wave rose in the figure. In the SJDF, stations were chosen at the midpoint between Vancouver Island and the north coast of the Olympic Peninsula starting at the location of buoy 46087 (SJDF1). At the entrance to the SJDF, the majority of the waves approach from the west and southwest, between 240° and 280°, and they have a maximum significant wave height of 8.67 m. The westward trend continues eastward in the SJDF, where a dramatic decrease in wave height occurs—decreasing to a range of 3 to 4 m in the mid-SJDF (SJDF3 and SJDF4) and below 3.5 m at the eastern end of the SJDF and near the mouth of Puget Sound (SJDF5/PS1). Some local wave generation from the southeast direction is observed at SJDF5/PS1; it was generated along the northern portion of the main basin in Puget Sound. Overall, the sea state in the SJDF is dominated by waves generated offshore in the Pacific Ocean and propagated into the strait.

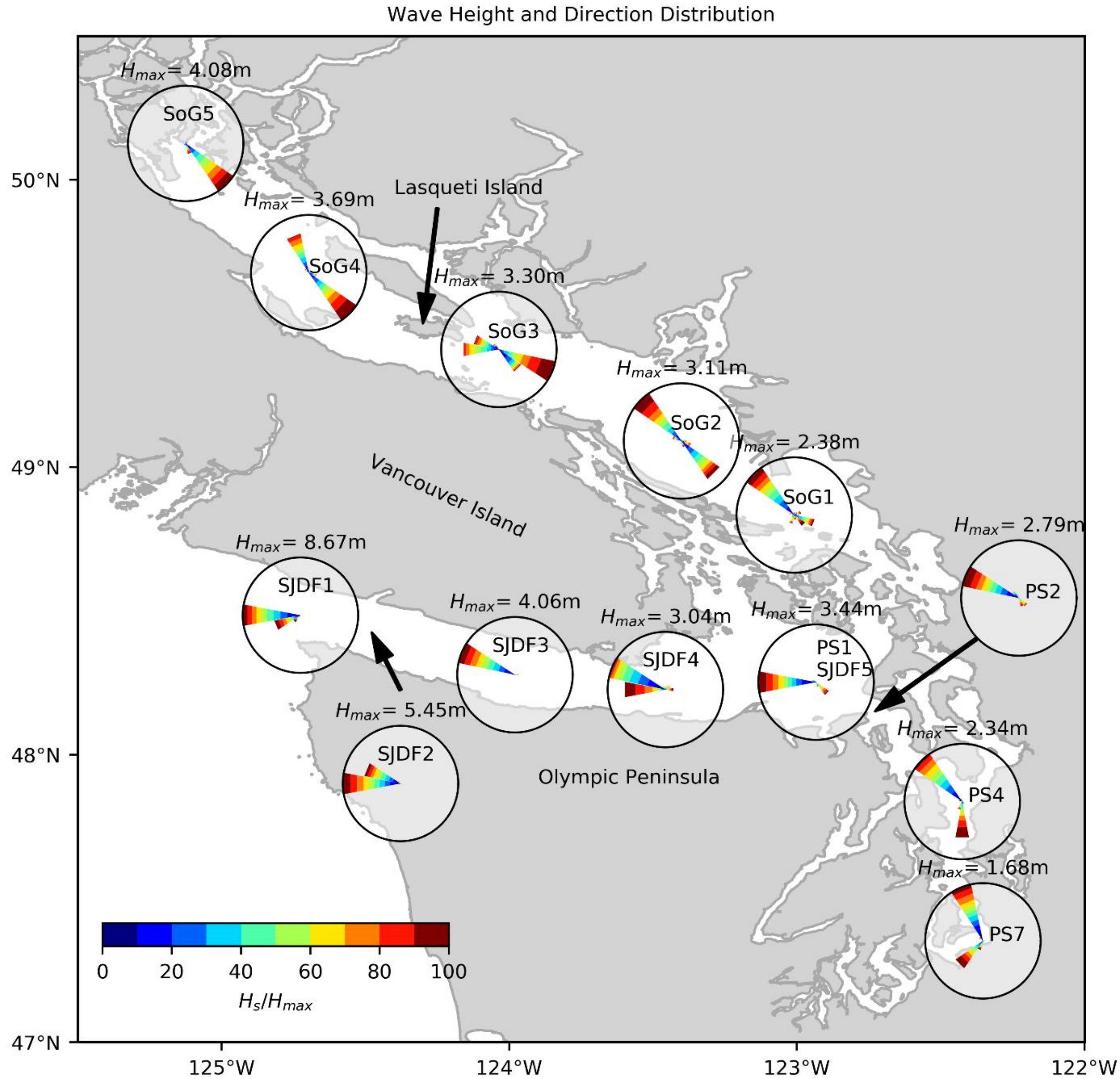

FIG. 8. Wave roses for selected locations during the analysis period of 2015.

Sea state in the SoG is more complicated than in the SJDF because of the influence of local wind field and the complex coastal geometry. Although waves can approach from either the northwest or the southeast in the majority of the strait (e.g., SoG2, SoG3, and SoG4), waves at the south end (SoG1) and north end (SoG5) of the

SoG are mainly propagated from the northwest and the southeast, respectively, because of the blocking effect of land boundaries. The maximum significant wave height in the SoG increases gradually from 2.68 m at SoG1 in the south to 4.08 m at SoG5 in the north. Interestingly, at SoG4 the larger waves approach from the southwest, similar to SoG3, even though the points are at opposite ends of Lasqueti Island. In the northern part of the SoG, dominant wave direction is from the southeast; while in the southern part of the SoG, large waves are generated by local wind forcing from the northwest.

Of the three main basins in the Salish Sea, the Puget Sound has the smallest waves. Wave magnitude in the Puget Sound shows a decreasing trend from the mouth (PS1) to the south end of the Sound (PS7). In the main channel at PS4, the majority of the waves approach from the northwest. However, the larger waves are those that approach from the south even though waves from that direction are prevalent only 33% of the time. The wave climate in the south Puget Sound is similar to that in the main channel. However, the waves in the south Puget Sound are generally smaller; the maximum significant wave height is 1.68 m at PS7 compared to 2.34 m at PS4 in the main channel.

Joint probability distributions of significant wave height and peak wave period show that at the entrance to the SJDF the majority of the waves have peak periods of over 10 s (FIG. *9*a). However, in the eastern portion of the SJDF and at the entrance to Puget Sound (FIG. *9*b, c), the wave energy at these bands (period >10 s) is dissipated quickly, and strong energy growth with a wave period of less than 5 s is evident. In the main basin of Puget Sound (FIG. *9*e), most of the waves have peak periods much less than 5 s. Interestingly, some long period energy makes it into the Puget Sound, but the significant wave heights of these longer waves (above 10 s) are very small (FIG. *9*d). The peak wave period was never above 10 s for SoG1 in the southern SoG, indicating that long waves entering the SJDF are not dominant at SoG1.

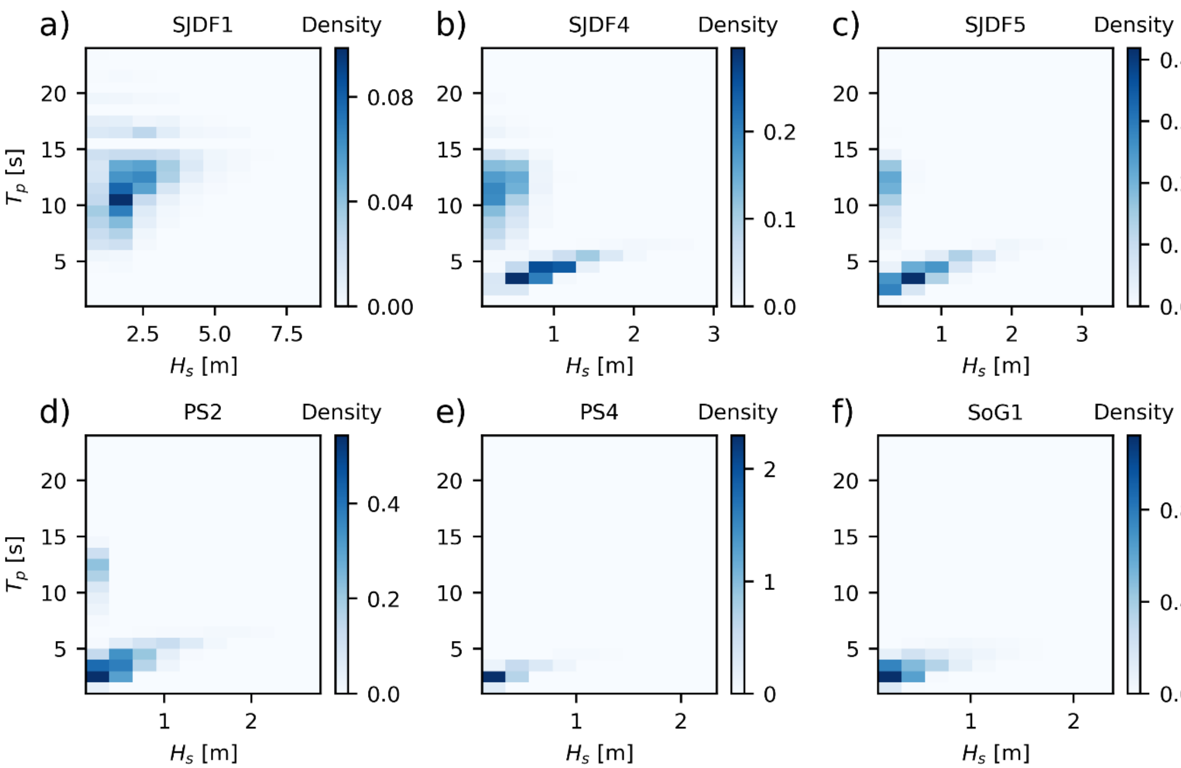

FIG. 9. Wave height and period distribution from the SJDF entrance to the Admiralty Inlet and south SoG. Note that the range of the abscissa is different for all subplots in order to show the wave height details. All joint probability distributions are normalized so that the total integral equals unity.

To analyze the wave climate, spectral partition output is obtained for year 2015 using the watershed algorithm of Hanson and Phillips (2001) as implemented in SWAN. To evaluate the sea states, the percentage of each partition that is forced by the wind is obtained. In this analysis, the partition is categorized as a wind-sea condition if at least 30% of the partition is forced by wind; otherwise, it is classified as swell. Additionally, if the significant wave height does not exceed 10 cm, the partition is not considered. No wave period cutoff is imposed for swell, so in this context swell does not necessarily mean long period waves. The percents of occurrences of pure wind, pure swell, and combined sea states at selected locations corresponding to FIG. 8 are presented in TABLE *4*. As shown in TABLE 4, nearly 89% of waves at the entrance of the SJDF are swell and 11% are combined wind-sea and swell. There is basically no contribution from pure wind-sea at SJDF1. In the east end of the SJDF and the mouth of Puget Sound, although pure swell is still dominant, the contribution of wind-driven waves increases, with approximately 15% being derived from pure windsea. Inside Puget Sound (PS4), sea state is dominated by locally wind-driven waves, at 82%, and only about 16% is contributed by pure swell.

TABLE 4. Percent occurrence of pure wind, pure swell, and combined sea states at selected locations. N is the number of events that exceeded the 10 cm significant wave height threshold. The location of these stations is shown in FIG. 8. The last column shows the percent of time the peak wave period is above 10 s.

Station	**N**	**Wind**	**Swell**	**Combined**	**%T_p>=10s**
SJDF1	8760	0.72	88.33	10.95	74.8
SJDF4	8634	14.55	49.10	36.35	40.4
SJDF5/PS1	6991	15.98	60.86	23.16	25.6
PS2	5735	31.40	57.96	10.64	16.3
PS4	1859	82.19	16.35	1.45	0
SoG1	4478	56.32	36.27	7.41	0

3.3 Seasonal Characteristics

Wave climate in the PNW experiences strong seasonality, typically characterized by a very calm sea in the summer months and large waves induced by windstorms in the winter months. However, the seasonality of the wave climate in the Salish Sea could be more complicated because of the influence of local wind effects and complex coastlines. This section describes the seasonal characteristics of wave climate in each of the three main basins in the Salish Sea separately.

To investigate the seasonality of wave climate in the Salish Sea, monthly averaged as well as 90th percentile significant wave heights at selected stations along the SJDF were analyzed based on the 5-year hindcast results (FIG. 10). The shaded band indicates the standard deviation. At the entrance to the SJDF (FIG. 10a), large waves are observed in the winter months; the 90th percentile wave height is over 4 m in December. The lowest wave height occurs in August when the 90th percentile wave height is just below 2 m. As waves propagate into the SJDF, wave heights drop dramatically (FIG. 10b), even just a short distance from the entrance (20 km between SJDF1 and SJDF2). Significant wave heights continue to decrease as waves propagate farther into the inland side of the SJDF (FIG. 10c-e). A distinct feature of wave climate in the eastern SJDF is that there are very little seasonal variations; the mean significant wave height is approximately 0.5 m throughout the year at SJDF4 and SJDF5 (see FIG. 10d, e). To compare the seasonal variations at different stations in the SJDF, distributions of normalized monthly averaged significant wave heights at all stations are plotted in FIG. 10f. The color codes of the stations are shown in FIG. 10g. Clearly, in the western SJDF (stations SJDF1 and SJDF2), the maximum and minimum wave heights occur in December and July, respectively. In contrast, maximum wave heights in the eastern SJDF (stations SJDF4 and SJDF5) occur in July. In the middle of the SJDF (SJDF3), transition of seasonality is observed—the peak wave height occurs in July, but the maximum wave height still occurs in December.

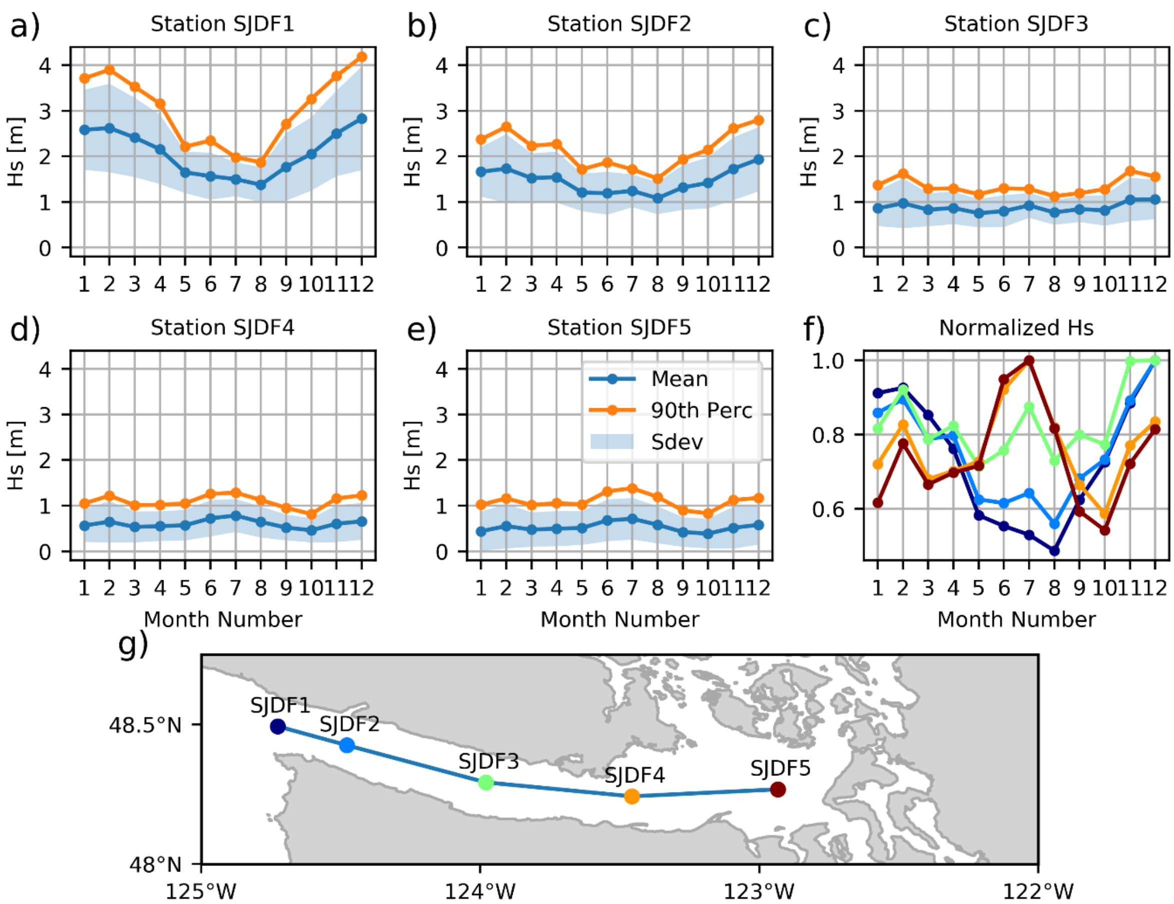

FIG. 10. (a-e) Monthly averaged significant wave height along the SJDF for selected stations. (f) Monthly averaged significant wave height normalized by the largest monthly wave height value for each station. (g) Station map. SJDF1 coincides with the location of buoy 46087.

In the SoG, the seasonality of wave climate shows a trend somewhat similar to the SJDF, except in a reverse direction (FIG. 11). In the southern SoG (FIG. 11a,b), although the maximum wave heights occur in December, a two-peak pattern in the summer and the winter is observed, similar to the wave climate in the eastern SJDF. Moving from the south to the north end of the SoG (FIG. 11c-e), waves become larger in the winter (December), and smaller in the summer, especially in July when the minimum wave height is reached at SoG5. The seasonal variations of wave climate at different stations in the SoG are more clearly shown in FIG. 11 by the normalized monthly wave heights.

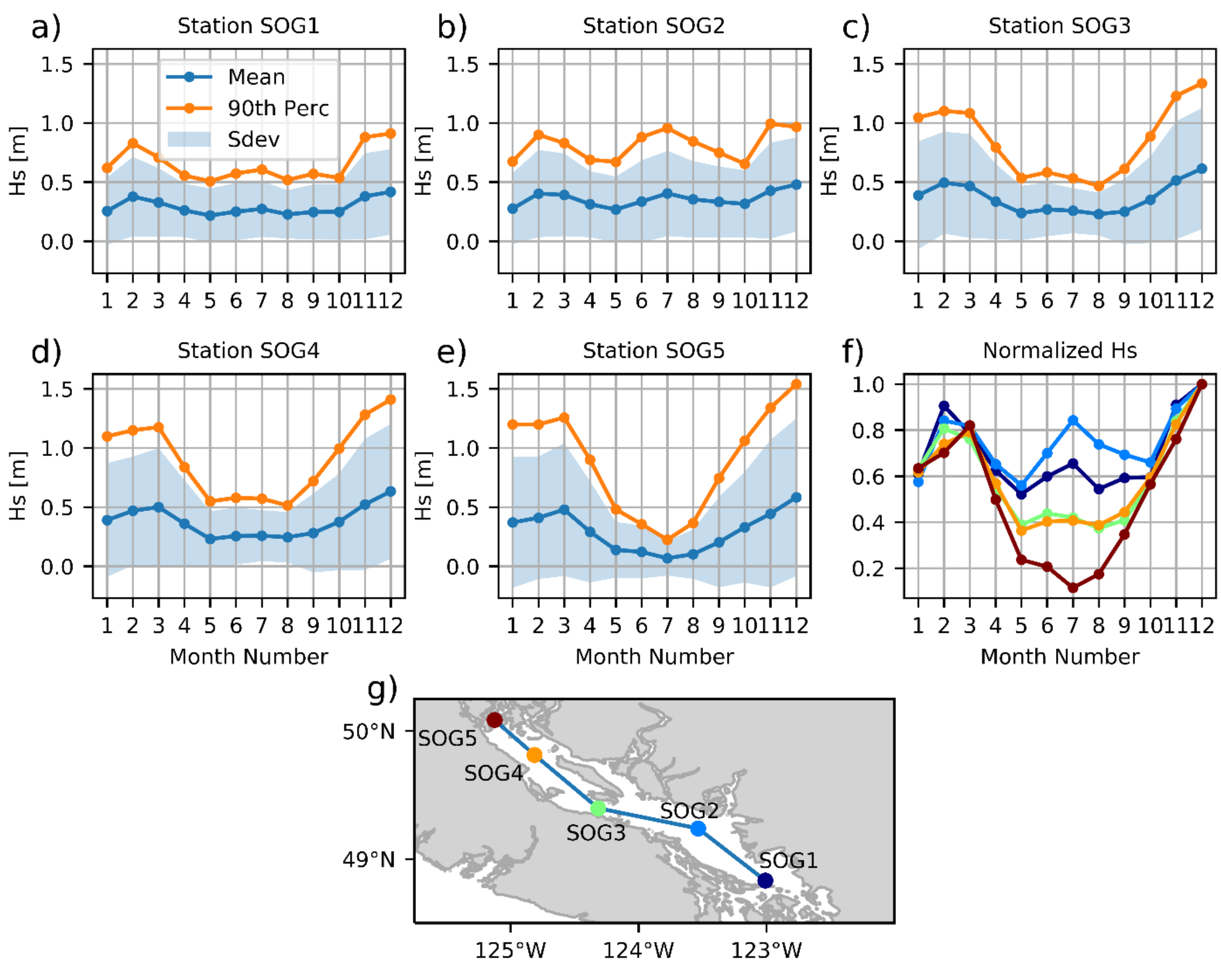

FIG. 11. (a-e) Monthly averaged significant wave height along the SoG for selected stations. (f) Monthly averaged significant wave height normalized by the largest monthly wave height value for each station. (g) Station map. Station SoG1 coincides with the location of buoy 46146.

The wave climate in Puget Sound is the mildest in the Salish Sea. Monthly averaged wave heights are well below 1 m in the entire Puget Sound, approximately 0.5 m near the entrance of the Sound (PS1 and 2), and below 0.25 m in the rest of the locations (PS3–PS8), especially in the south Puget Sound where wave height is close to zero throughout the year (FIG. 12). Unlike the SJDF and SoG, wave climate in Puget Sound shows very little seasonality, likely due to the limited fetch for full wave growth in any of the sub-basins in Puget Sound. No distinct seasonal patterns in wave climate are found inside Puget Sound. Although normalized monthly averaged wave heights indicate that the maximum and the minimum wave heights in the south Puget Sound (PS8) occur in the winter and the summer, such a seasonality is insignificant because waves are extremely small (FIG. 12h).

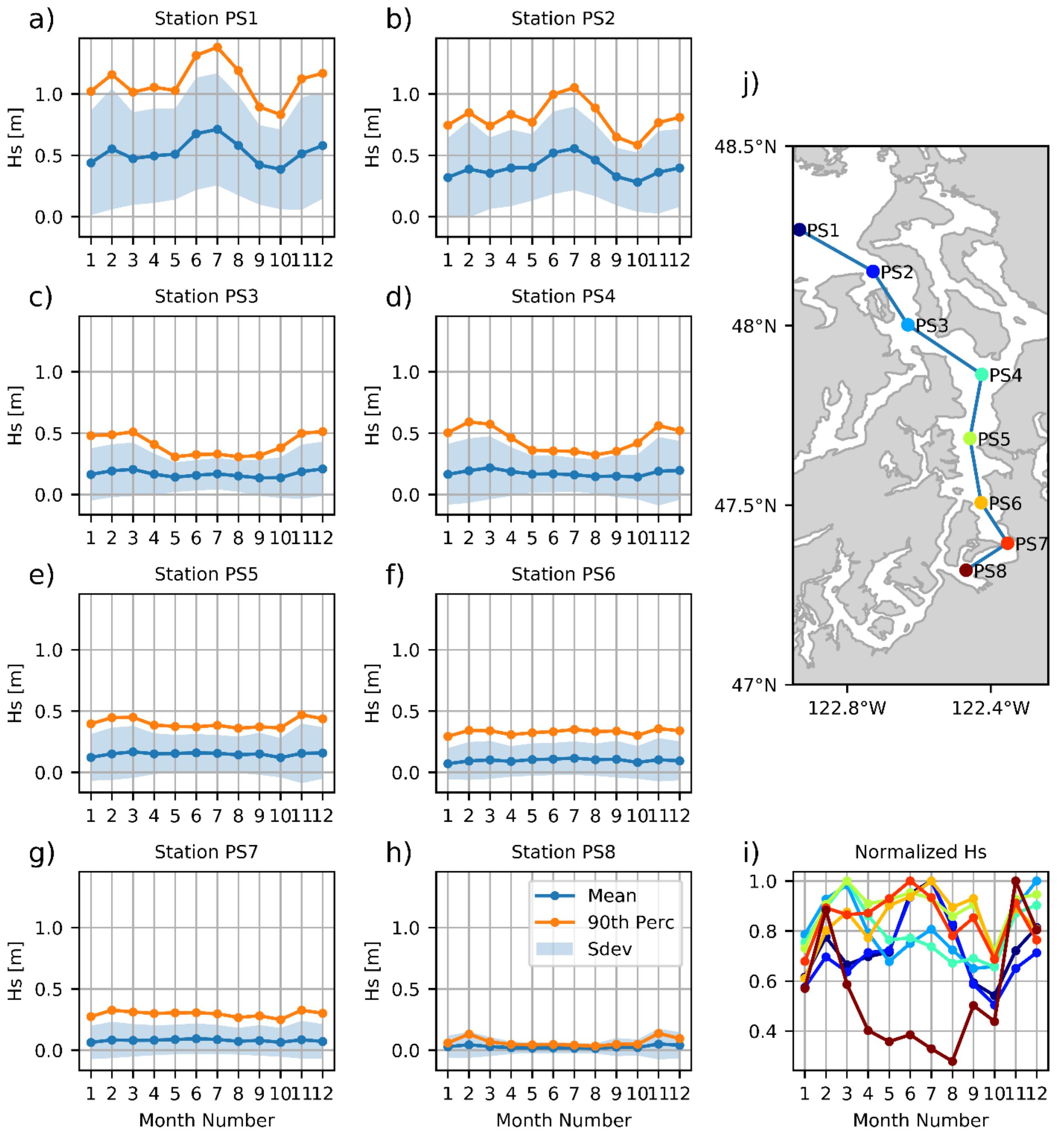

FIG. 12. (a-i) Monthly averaged significant wave height along the main basin of Puget Sound for selected stations. (j) Station map. PS1 and SJDF5 are the same station.

4 Conclusions

A high-resolution UnSWAN wave model was developed to simulate wave climate in the Salish Sea. The Salish Sea wave model was driven by wave spectral output from a three-level nested WW3 model and wind forcing from a high-resolution regional WRF hindcast. Wind sensitivity analysis indicates that while the 0.5° resolution CFSR wind is sufficient for driving wave hindcasting in the open ocean, high-resolution and accurate wind forcing is necessary to drive the Salish Sea wave model due to the complexity of the model domain. This study demonstrates that the high-resolution wind field obtained from the 6 km resolution WRF hindcast can significantly improve wave hindcast accuracy in the Salish Sea. Satisfactory model validation at four wave buoys demonstrates that the wave model is able to accurately simulate the wave climate in the Salish Sea. Sea states in three main basins of the Salish Sea were analyzed based on 5-year wave hindcast results.

Waves in the SJDF are dominated by swells with a peak period of over 10 s, which are generated remotely in the Pacific Ocean and propagated into the strait. Once they enter the SJDF, swells dissipate significantly from the west to the east side of the strait. Different from waves in the SJDF, waves in the SoG and Puget Sound are dominated by local wind fields in the direction oriented to the main channel. In particular, waves in Puget Sound are small and primarily contributed by wind-sea; peak periods are generally less than 5 s and maximum significant wave heights are less than 2.0 m. The seasonality of wave climate can be very different depending on the locations evaluated in the Salish Sea. In the western SJDF, which is strongly influenced by swells propagated from the Pacific Ocean, waves are the largest in the winter and smallest in the summer. However, in the eastern SJDF and the southern SoG, wave climates show a two-peak seasonal feature—maximum wave heights occur either in the summer or winter.

The 5-year high-resolution wave hindcast conducted in this study provides first of their kind wave climate data for the Salish Sea. These data will be useful in better understanding the role of wave climate in coastal processes in the Salish Sea, such as sea-surface mixing, wave energy assessment, wave-current interaction, and nearshore sediment transport. The comprehensive wave data set is also important in assessing the coastal hazards related to sea level rise and extreme wave actions in the Salish Sea.

5 Acknowledgements

This project was funded in part by the U.S. Environmental Protection Agency under assistance agreement PC-01J22301 through the Washington Department of Fish and Wildlife. The Weather Research and Forecasting (WRF) climate simulation was supported by the Strategic Environmental Research and Development Program under contract RC-2546 and by the U.S. Department of Energy, Office of Energy Efficiency and Renewable Energy, Water Power Technologies Office. The WRF simulation was performed using the facilities of the PNNL Institutional Computing Center and the National Energy Research Supercomputing Center, which is supported by the DOE Office of Science under contract DE-AC02-05CH11231. The UnSWAN simulation was also conducted using the facilities of the PNNL Institutional Computing Center.

Declarations of interest: none

APPENDIX A: Model Performance Metrics

To quantitatively evaluate the model performance in simulating the wave climate, five statistics were computed to compare model results with measurements. The root-mean-square-error ($RMSE$) is defined as:

$$RMSE = \sqrt{\frac{\sum_{i=1}^{N}(P_i - M_i)^2}{N}}$$

where N is the number of observations, M_i is the measured value, and P_i is the model generated value.

The percent error (PE) is defined as:

$$PE = \frac{100}{N}\sum_{i=1}^{N}\frac{P_i - M_i}{M_i}$$

The scatter index (SI) is the $RMSE$ normalized by the average measurement:

$$SI = \frac{RMSE}{\overline{M}}$$

The scatter index helps put the $RMSE$ values into context when comparing regions of large wave heights with regions of small wave heights.

The bias is defined as:

$$Bias = \frac{\sum_{i=1}^{N} P_i - M_i}{N}$$

Finally, the linear correlation coefficient (R) is a measure of the linear relationship between the predictions and the measurements from 0 to 1, where 1 is a perfect fit:

$$R = \frac{\sum_{i=1}^{N}\left(P_i - \overline{P}\right)^2\left(M_i - \overline{M}\right)^2}{\sqrt{\left(\sum_{i=1}^{N}\left(M_i - \overline{M}\right)^2\right)\left(\sum_{i=1}^{N}\left(P_i - \overline{P}\right)^2\right)}}$$

References

Akpinar, A., Bingolbali, B., and Van Vledder, G. P., 2016, Wind and wave characteristics in the Black Sea based on the SWAN wave model forced with the CFSR winds: Ocean Engineering, v. 126, p. 276-298.

Alari, V., Raudsepp, U., and Kouts, T., 2008, Wind wave measurements and modelling in Kudema Bay, Estonian Archipelago Sea: Journal of Marine Systems, v. 74, p. S30-S40.

Albarakati, A. M. A., and Aboobacker, V. M., 2018, Wave transformation in the nearshore waters of Jeddah, west coast of Saudi Arabia: Ocean Engineering, v. 163, p. 599-608.

Allan, J. C., and Komar, P. D., 2002, Extreme storms on the Pacific Northwest coast during the 1997-98 El Nino and 1998-99 La Nina: Journal of Coastal Research, v. 18, no. 1, p. 175-193.

Amante, C., and Eakins, B., 2009, ETOPO1 1 arc-minute global relief model: procedures, data sources and analysis.: NATIONAL OCEANIC AND ATMOSPHERIC ADMINISTRATION, National Environmental Satellite, Data, and Information Service, National Geophysical Data Center Marine Geology and Geophysics Division.

Anselmi-Molina, C. M., Canals, M., Morell, J., Gonzalez, J., Capella, J., and Mercado, A., 2012, Development of an Operational Nearshore Wave Forecast System for Puerto Rico and the US Virgin Islands: Journal of Coastal Research, v. 28, no. 5, p. 1049-1056.

Battjes, J. A., and Janssen, J., 1978, Energy loss and set-up due to breaking of random waves, Coastal Engineering 1978, p. 569-587.

Bento, A. R., Martinho, P., and Soares, C. G., 2015, Numerical modelling of the wave energy in Galway Bay: Renewable Energy, v. 78, p. 457-466.

Beudin, A., Ganju, N. K., Defne, Z., and Aretxabaleta, A. L., 2017, Physical response of a back-barrier estuary to a post-tropical cyclone: Journal of Geophysical Research-Oceans, v. 122, no. 7, p. 5888-5904.

Bolanos-Sanchez, R., Sanchez-Arcilla, A., and Cateura, J., 2007, Evaluation of two atmospheric models for wind-wave modelling in the NW Mediterranean: Journal of Marine Systems, v. 65, no. 1-4, p. 336-353.

Campos, R. M., Alves, J. H. G. M., Soares, C. G., Guimaraes, L. G., and Parente, C. E., 2018, Extreme wind-wave modeling and analysis in the south Atlantic ocean: Ocean Modelling, v. 124, p. 75-93.

Campos, R. M., and Soares, C. G., 2016, Comparison and assessment of three wave hindcasts in the North Atlantic Ocean: Journal of Operational Oceanography, v. 9, no. 1, p. 26-44.

Carignan, K. S., McLean, S. J., Eakins, B. W., Beasley, L., Love, M. R., and Sutherland, M., 2014, Digital Elevation Model of Puget Sound, Washington: Procedures, Data Sources, and Analysis.: NOAA National Geophysical Data Center.

Cavaleri, L., and Rizzoli, P. M., 1981, Wind Wave Prediction in Shallow-Water - Theory and Applications: Journal of Geophysical Research-Oceans, v. 86, no. Nc11, p. 961-973.

Chen, X. D., Leung, L. R., Gao, Y., Liu, Y., Wigmosta, M., and Richmond, M., 2018, Predictability of Extreme Precipitation in Western US Watersheds Based on Atmospheric River Occurrence, Intensity, and Duration: Geophysical Research Letters, v. 45, no. 21, p. 11693-11701.

Chen, Y., Wai, O. W. H., and Li, Y. S., 2003, Numerical model for wave refraction-diffraction near Pearl River estuary, China: Journal of Waterway Port Coastal and Ocean Engineering, v. 129, no. 6, p. 260-269.

Cheng, T. K., Hill, D. F., Beamer, J., and Garcia-Medina, G., 2015, Climate change impacts on wave and surge processes in a Pacific Northwest (USA) estuary: Journal of Geophysical Research-Oceans, v. 120, no. 1, p. 182-200.

Crosby, S. C., Cornuelle, B. D., O'Reilly, W. C., and Guza, R. T., 2017, Assimilating Global Wave Model Predictions and Deep-Water Wave Observations in Nearshore Swell Predictions: Journal of Atmospheric and Oceanic Technology, v. 34, no. 8, p. 1823-1836.

Crosby, S. C., O'Reilly, W. C., and Guza, R. T., 2016, Modeling Long-Period Swell in Southern California: Practical Boundary Conditions from Buoy Observations and Global Wave Model Predictions: Journal of Atmospheric and Oceanic Technology, v. 33, no. 8, p. 1673-1690.

Dupuis, K. W., and Anis, A., 2013, Observations and Modeling of Wind Waves in a Shallow Estuary: Galveston Bay, Texas: Journal of Waterway Port Coastal and Ocean Engineering, v. 139, no. 4, p. 314-325.

EPRI, 2011, Mapping and Assessment of the United States Ocean Wave Energy Resource: Electric Power Research Institute.

Finlayson, D. P., 2005, Combined bathymetry and topography of the Puget Lowland, Washington State, University of Washington.

Gao, Y., Leung, L. R., Zhao, C., and Hagos, S., 2017, Sensitivity of US summer precipitation to model resolution and convective parameterizations across gray zone resolutions: Journal of Geophysical Research-Atmospheres, v. 122, no. 5, p. 2714-2733.

Garcia-Medina, G., Ozkan-Haller, H. T., and Ruggiero, P., 2014, Wave resource assessment in Oregon and southwest Washington, USA: Renewable Energy, v. 64, p. 203-214.

García-Medina, G., Özkan-Haller, H. T., and Ruggiero, P., 2014, Wave resource assessment in Oregon and southwest Washington, USA: Renewable Energy, v. 64, p. 203-214.

García-Medina, G., Özkan-Haller, H. T., Ruggiero, P., and Oskamp, J., 2013, An Inner-Shelf Wave Forecasting System for the U.S. Pacific Northwest: Weather and Forecasting, v. 28, no. 3, p. 681-703.

Gorman, R. M., and Neilson, C. G., 1999, Modelling shallow water wave generation and transformation in an intertidal estuary: Coastal Engineering, v. 36, no. 3, p. 197-217.

Guillou, N., and Chapalain, G., 2015, Numerical modelling of nearshore wave energy resource in the Sea of Iroise: Renewable Energy, v. 83, p. 942-953.

Hanson, J. L., and Phillips, O. M., 2001, Automated analysis of ocean surface directional wave spectra: Journal of atmospheric and oceanic technology, v. 18, no. 2, p. 277-293.

Hanson, J. L., Tracy, B. A., Tolman, H. L., and Scott, R. D., 2009, Pacific Hindcast Performance of Three Numerical Wave Models: Journal of Atmospheric and Oceanic Technology, v. 26, no. 8, p. 1614-1633.

Harr, P. A., Elsberry, R. L., and Hogan, T. F., 2000, Extratropical transition of tropical cyclones over the western North Pacific. Part II: The impact of midlatitude circulation characteristics: Monthly Weather Review, v. 128, no. 8, p. 2634-2653.

Hasselmann, K., Barnett, T., Bouws, E., Carlson, H., Cartwright, D., Enke, K., Ewing, J., Gienapp, H., Hasselmann, D., and Kruseman, P., 1973, Measurements of wind-wave growth and swell decay during the Joint North Sea Wave Project (JONSWAP): Ergänzungsheft 8-12.

Hasselmann, S., Hasselmann, K., Allender, J. H., and Barnett, T. P., 1985, Computations and Parameterizations of the Nonlinear Energy-Transfer in a Gravity-Wave Spectrum .2. Parameterizations of the Nonlinear Energy-Transfer for Application in Wave Models: Journal of Physical Oceanography, v. 15, no. 11, p. 1378-1391.

Janssen, P. A. E. M., 1989, Wave-Induced Stress and the Drag of Air-Flow over Sea Waves: Journal of Physical Oceanography, v. 19, no. 6, p. 745-754.

-, 1991, Quasi-Linear Theory of Wind-Wave Generation Applied to Wave Forecasting: Journal of Physical Oceanography, v. 21, no. 11, p. 1631-1642.

Kita, Y., Waseda, T., and Webb, A., 2018, Development of waves under explosive cyclones in the Northwestern Pacific: Ocean Dynamics, v. 68, no. 10, p. 1403-1418.

Komen, G. J., Hasselmann, S., and Hasselmann, K., 1984, On the Existence of a Fully-Developed Wind-Sea Spectrum: Journal of Physical Oceanography, v. 14, no. 8, p. 1271-1285.

Lavidas, G., Venugopal, V., and Friedrich, D., 2017, Sensitivity of a numerical wave model on wind re-analysis datasets: Dynamics of Atmospheres and Oceans, v. 77, p. 1-16.

Lin, W. Q., Sanford, L. P., and Suttles, S. E., 2002, Wave measurement and modeling in Chesapeake bay: Continental Shelf Research, v. 22, no. 18-19, p. 2673-2686.

Martin, J. E., Grauman, R. D., and Marsili, N., 2001, Surface cyclolysis in the North Pacific Ocean. Part I: A synoptic climatology: Monthly Weather Review, v. 129, no. 4, p. 748-765.

Mass, C., and Dotson, B., 2010, Major Extratropical Cyclones of the Northwest United States: Historical Review, Climatology, and Synoptic Environment: Monthly Weather Review, v. 138, no. 7, p. 2499-2527.

Mesinger, F., DiMego, G., Kalnay, E., Mitchell, K., Shafran, P. C., Ebisuzaki, W., Jovic, D., Woollen, J., Rogers, E., Berbery, E. H., Ek, M. B., Fan, Y., Grumbine, R., Higgins, W., Li, H., Lin, Y., Manikin, G., Parrish, D., and Shi, W., 2006, North American regional reanalysis: Bulletin of the American Meteorological Society, v. 87, no. 3, p. 343-360.

Mesquita, M. D. S., Atkinson, D. E., and Hodges, K. I., 2010, Characteristics and Variability of Storm Tracks in the North Pacific, Bering Sea, and Alaska: Journal of Climate, v. 23, no. 2, p. 294-311.

Morim, J., Cartwright, N., Etemad-Shahidi, A., Strauss, D., and Hemer, M., 2016, Wave energy resource assessment along the Southeast coast of Australia on the basis of a 31-year hindcast: Applied Energy, v. 184, p. 276-297.

Mulligan, R. P., Bowen, A. J., Hay, A. E., van der Westhuysen, A. J., and Battjes, J. A., 2008, Whitecapping and wave field evolution in a coastal bay: Journal of Geophysical Research-Oceans, v. 113, no. C3.

Nayak, S., Bhaskaran, P. K., Venkatesan, R., and Dasgupta, S., 2013, Modulation of local wind-waves at Kalpakkam from remote forcing effects of Southern Ocean swells: Ocean Engineering, v. 64, p. 23-35.

Niroomandi, A., Ma, G. F., Ye, X. Y., Lou, S., and Xue, P. F., 2018, Extreme value analysis of wave climate in Chesapeake Bay: Ocean Engineering, v. 159, p. 22-36.

O'Dea, A., Haller, M. C., and Ozkan-Haller, H. T., 2018, The impact of wave energy converter arrays on wave-induced forcing in the surf zone: Ocean Engineering, v. 161, p. 322-336.

Robertson, B. R., Hiles, C. E., and Buckham, B. J., 2014, Characterizing the near shore wave energy resource on the west coast of Vancouver Island, Canada: Renewable energy, v. 71, p. 665-678.

Rusu, E., Goncalves, M., and Soares, C. G., 2011a, Evaluation of the wave transformation in an open bay with two spectral models: Ocean Engineering, v. 38, no. 16, p. 1763-1781.

Rusu, L., Bernardino, M., and Soares, C. G., 2011b, Modelling the influence of currents on wave propagation at the entrance of the Tagus estuary: Ocean Engineering, v. 38, no. 10, p. 1174-1183.

Saha, S., Moorthi, S., Pan, H. L., Wu, X. R., Wang, J. D., Nadiga, S., Tripp, P., Kistler, R., Woollen, J., Behringer, D., Liu, H. X., Stokes, D., Grumbine, R., Gayno, G., Wang, J., Hou, Y. T., Chuang, H. Y., Juang, H. M. H., Sela, J., Iredell, M., Treadon, R., Kleist, D., Van Delst, P., Keyser, D., Derber, J., Ek, M., Meng, J., Wei, H. L., Yang, R. Q., Lord, S., Van den Dool, H., Kumar, A., Wang, W. Q., Long, C., Chelliah, M., Xue, Y., Huang, B. Y., Schemm, J. K., Ebisuzaki, W., Lin, R., Xie, P. P., Chen, M. Y., Zhou, S. T., Higgins, W., Zou, C. Z., Liu, Q. H., Chen, Y., Han, Y., Cucurull, L., Reynolds, R. W., Rutledge, G., and Goldberg, M., 2010, The Ncep Climate Forecast System Reanalysis: Bulletin of the American Meteorological Society, v. 91, no. 8, p. 1015-1057.

Sartini, L., Weiss, J., Prevosto, M., Bulteau, T., Rohmer, J., and Maisondieu, C., 2018, Spatial analysis of extreme sea states affecting Atlantic France: a critical assessment of the RFA approach: Ocean Modelling, v. 130, p. 48-65.

Semedo, A., Vettor, R., Breivik, O., Sterl, A., Reistad, M., Soares, C. G., and Lima, D., 2015, The wind sea and swell waves climate in the Nordic seas: Ocean Dynamics, v. 65, no. 2, p. 223-240.

Skamarock, W. C., Klemp, J. B., Dudhia, J., Gill, D. O., Barker, D. M., Duda, M. G., Huang, X., Wang, W., and Powers, J. G., 2008, A description of the advanced research WRF version 3: Natl. Cent. for Atmos. Res., NCAR Tech. Note, NCAR/TN-475 + STR.

Stopa, J. E., and Cheung, K. F., 2014, Intercomparison of wind and wave data from the ECMWF Reanalysis Interim and the NCEP Climate Forecast System Reanalysis: Ocean Modelling, v. 75, p. 65-83.

SWAN Team, 2017, SWAN: User Manual, Cycle III Version 41.10: Delft University of Technology. The Netherlands.

Tolman, H. L., and WAVEWATCH III Development Group, 2014, User Manual and System Documentation of Wavewatch III Version 4.18, College Park, MD, 20740, National Oceanic and Atmospheric Administration, National Weather Service, 311 p.:

Umesh, P. A., Swain, J., and Balchand, A. N., 2018, Inter-comparison of WAM and WAVEWATCH-III in the North Indian Ocean using ERA-40 and QuikSCAT/NCEP blended winds: Ocean Engineering, v. 164, p. 298-321.

Wang, T. P., and Yang, Z. Q., 2017, A modeling study of tidal energy extraction and the associated impact on tidal circulation in a multi-inlet bay system of Puget Sound: Renewable Energy, v. 114, p. 204-214.

Wu, W.-C., Yang, Z., and Wang, T., 2018, Wave Resource Characterization Using an Unstructured Grid Modeling Approach: Energies, v. 11, no. 3, p. 605.

Xu, F. M., Perrie, W., Zhang, J. L., Song, Z. Y., and Toulany, B., 2005, Simulation of typhoon-driven waves in the Yangtze Estuary with multiple-nested wave models: China Ocean Engineering, v. 19, no. 4, p. 613-624.

Yang, Z. Q., and Khangaonkar, T., 2010, Multi-scale modeling of Puget Sound using an unstructured-grid coastal ocean model: from tide flats to estuaries and coastal waters: Ocean Dynamics, v. 60, no. 6, p. 1621-1637.

Yang, Z. Q., Neary, V. S., Wang, T. P., Gunawan, B. D., Dallman, A. R., and Wu, W. C., 2017, A wave model test bed study for wave energy resource characterization: Renewable Energy, v. 114, p. 132-144.

Yang, Z. Q., and Wang, T. P., 2015, Responses of estuarine circulation and salinity to the loss of intertidal flats - A modeling study: Continental Shelf Research, v. 111, p. 159-173.

Yang, Z. Q., Wu, W. C., Wang, T., and Castrucci, L., 2018, High-Resolution Regional Wave Hindcast for the U.S. West Coast Pacific Northwest National Laboratory, PNNL-28107.